Journal of Global Environment Engineering, Vol. 6, pp. 13-31, 2000

RADIATIVE TRANSFER MODEL FOR SATELLITE REMOTE SENSING OF OCEAN COLORS IN COASTAL ZONES

Hiroshi Kobayashi [1]
Sachio Ohta [2]
Naoto Murao [3]
Harukuni Tachibana [4]
Sadamu Yamagata [5]

Abstract

A radiative transfer model for a coupled atmosphere-ocean system was developed for satellite remote sensing of coastal pollution to estimate water-leaving radiance from polluted sea surfaces. The optical properties of suspended substances in the ocean such as phytoplankton (*Skeletonema costatum* and *Heterosigma akashiwo*), detritus, submicron particles, and inorganic particles were measured or estimated. The equation of radiative transfer in the coupled atmosphere-ocean system was solved by using the invariance imbedding method. The water-leaving radiance in clear and Case II waters, turbid waters with soil particles, and red tide waters, were calculated. It was possible to estimate the soil particle concentration of water by using the ratio of the upward radiance at different wavelengths with satellite remote sensing using the Landsat TM. However, estimating the red tide phytoplankton concentration was difficult, because the water-leaving radiance varies little with phytoplankton concentration for sensitivity of the TM, and is affected by assumed amounts of detritus.

KEYWORDS: *equation of radiative transfer, coastal pollution, discharge of soil particle, red tide*

1. Introduction

In the control of water pollution like red tides and soil discharges in coastal zones it is necessary to make a quantitative determination of turbidity. Satellite remote sensing is considered to be able to provide observation of extensive areas. The solar radiation penetrating to the ocean is affected by Rayleigh scattering of seawater molecules, Mie scattering of suspended particles, and absorption of dissolved and suspended substances before the radiation leaves the sea surface to return to the atmosphere. The water-leaving radiance, i.e., the ocean color, varies with kind and quantity of

1 D.Eng., Instructor, Dept.of Ecosocial System Engineering, Yamanashi Univ., Koufu 400-8511, Japan
2 D.Sci., Prof., Div.of Environ. and Resource Engineering, Hokkaido Univ., Sapporo 060-8628, Japan
3 D.Eng., Associate Prof., Div.of Environ. and Resource Engineering, Hokkaido Univ.
4 D.Eng., Associate Prof., Div.of Environ. and Resource Engineering, Hokkaido Univ.
5 D.Eng., Instructor, Div.of Environ. and Resource Engineering, Hokkaido Univ.

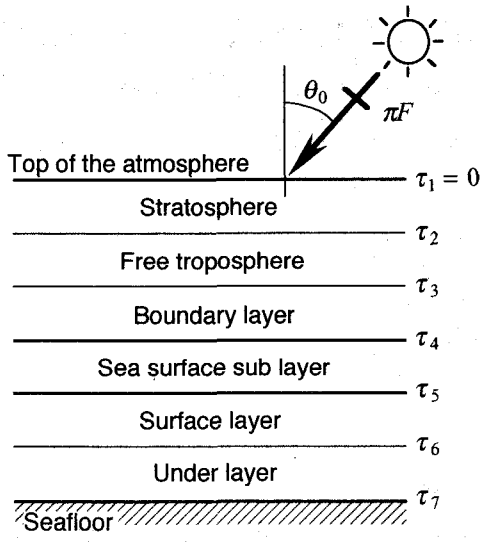

Figure 1. Radiative transfer model for a coupled atmosphere-ocean system.

particles in the water, dark blue in clear waters, green in coastal waters, brown and red in waters where red tides have occurred. It may then, be possible to determine pollutant concentrations by observations of ocean color.

There are two approaches to obtain the relationship between pollutant concentration and water-leaving radiance: statistical and optical modeling methods. In statistical methods, regression lines are calculated by using measurements of the water-leaving radiance and the pollutant concentration at many sites across the ocean. The relationship is then applied to estimate the pollutant concentrations at other places on the other days. In the optical modeling method, the relationship between pollutant concentration and water-leaving radiance is calculated theoretically by solving an equation of radiative transfer with given optical properties of dissolved and suspended matter and seawater. In the coastal zone, the kinds and concentration of phytoplankton, inorganic particles, and dissolved organic matter in the ocean vary temporally and spatially and it is difficult to determine a unique regression line.

This study uses the optical modeling method, a radiative transfer model for the coupled atmosphere-ocean system, and discusses an algorithm for determining concentrations of soil particles and red tide phytoplankton.

2. Radiative Transfer Model for a Coupled Atmosphere-Ocean System

2.1 Radiative Transfer Model

Figure 1 considers a plane-parallel layer model of the atmosphere-ocean system where τ is the optical thickness. The equation for the transfer of solar radiation through a plane-parallel medium is,

$$\mu \frac{dI(\tau;\mu,\varphi)}{d\tau} = I(\tau;\mu,\varphi) - \frac{1}{2}\int_0^{2\pi}\int_{-1}^{1} P(\tau;\mu,\varphi;\mu',\varphi')I(\tau;\mu',\varphi')\,d\mu' d\varphi' - \frac{1}{4}F\exp(-\tau/\mu_0)P(\tau;\mu,\varphi;\mu_0,\varphi_0), \quad (1)$$

where $I(\tau;\mu,\varphi)$ is the intensity at the optical thickness τ in the direction (μ,φ), μ is the cosine

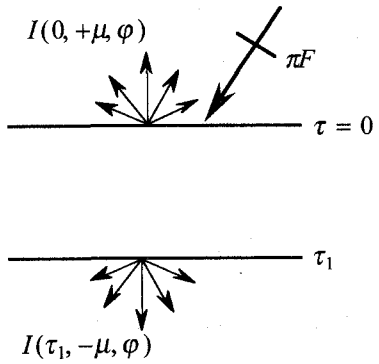

Figure 2. Schematic diagram of scattering and transmission functions

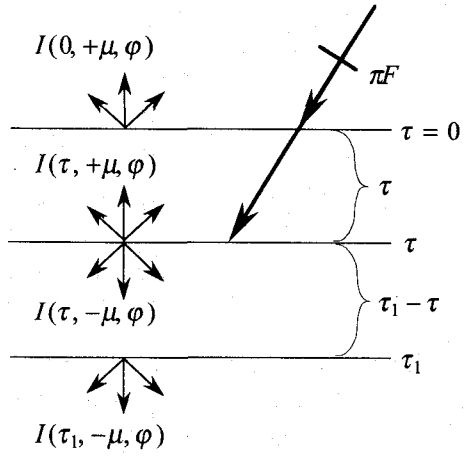

Figure 3. Schematic diagram of connection with two different layeres on the imvariance imbedding method

of the nadir angle, and φ is the azimuthal angle. The incident solar radiation flux is $\pi \mathrm{F}$, μ_0 is the cosine of solar zenith angle, and φ_0 is the solar azimuthal angle. The phase function $P(\tau;\mu,\varphi;\mu',\varphi')$ gives the portion of radiation scattered to (μ,φ) from (μ',φ').

The invariance imbedding method (Chandrasekhar, 1960) was used to solve the radiative transfer equation in the coupled atmosphere-ocean system. The basic concept of invariance imbedding is that the scattering and diffuse transmittance properties of a layer are obtained by the scattering and diffuse transmittance properties of the internal layers. Next a plane-parallel layer such as in Figure 2 is considered, a parallel beam of solar radiation flux $\pi \mathrm{F}$ incident on the plane-parallel layer. The intensities reflected and transmitted to the layer are given by

$$I(0,+\mu,\varphi) = \frac{F}{4\mu} S(\tau_1;\mu,\varphi;\mu_0,\varphi_0), \quad (2)$$

$$I(\tau_1,-\mu,\varphi) = \frac{F}{4\mu} T(\tau_1;\mu,\varphi;\mu_0,\varphi_0), \quad (3)$$

where $S(\tau_1;\mu,\varphi;\mu_0,\varphi_0)$ and $T(\tau_1;\mu,\varphi;\mu_0,\varphi_0)$ are the *scattering* and *transmission functions*. These functions are determined from the optical properties of various components in the layer using the discrete ordinates method (e.g. Stamnes, 1986) while accounting for multiple scattering processes. In incident radiation with diffuse light of intensity $I_{inc}(\mu',\varphi')$, the reflected and the transmitted intensities are given by

$$I_{ref}(0,+\mu,\varphi) = \frac{1}{4\pi\mu}\int_0^1\int_0^{2\pi} S(\tau_1;\mu,\varphi;\mu',\varphi') I_{inc}(\mu',\varphi')\, d\varphi' d\mu', \quad (4)$$

$$I_{trans}(\tau_1,-\mu,\varphi) = \frac{1}{4\pi\mu}\int_0^1\int_0^{2\pi} T(\tau_1;\mu,\varphi;\mu',\varphi') I_{inc}(\mu',\varphi')\, d\varphi' d\mu'. \quad (5)$$

Here two plane-parallel layers as in Figure 3 are considered. The upward intensity $I(0, +\mu, \varphi)$ at the top of the layers is given by

$$\begin{aligned} I(0, +\mu, \varphi) &= \frac{F}{4\mu} S(\tau_1; \mu, \varphi; \mu_0, \varphi_0) \\ &= \frac{F}{4\mu} S(\tau; \mu, \varphi; \mu_0, \varphi_0) \\ &+ \exp(-\tau / \mu) I(\tau, +\mu, \varphi) \\ &+ \frac{1}{4\pi\mu} \int_0^1 \int_0^{2\pi} T(\tau; \mu, \varphi; \mu', \varphi') I(\tau, +\mu', \varphi') \, d\varphi' d\mu'. \end{aligned} \tag{6}$$

The three terms on the right-hand side represent, (1) the upper layer reflected radiation of the incident solar flux, (2) the direct transmission of the diffusion intensity $I(\tau;+\mu,\varphi)$ in the direction $(+\mu,\varphi)$, and (3) the diffuse transmission of the diffusion intensity on τ from below.

In the same manner, the intensity $I(\tau_1;-\mu,\varphi)$ in the downward direction at the bottom of the layers is given by

$$\begin{aligned} I(\tau_1, -\mu, \varphi) &= \frac{F}{4\mu} T(\tau_1; \mu, \varphi; \mu_0, \varphi_0) \\ &= \frac{F}{4\mu} \exp(-\tau / \mu_0) T(\tau_1 - \tau; \mu, \varphi; \mu_0, \varphi_0) \\ &+ \exp(-(\tau_1 - \tau) / \mu) I(\tau, -\mu, \varphi) \\ &+ \frac{1}{4\pi\mu} \int_0^1 \int_0^{2\pi} T(\tau_1 - \tau; \mu, \varphi; \mu', \varphi') I(\tau, -\mu', \varphi') \, d\varphi' d\mu'. \end{aligned} \tag{7}$$

The intensities at the boundary between two layers in the upward and downward directions are given by

$$\begin{aligned} I(\tau, +\mu, \varphi) &= \frac{F}{4\mu} \exp(-\tau / \mu_0) S(\tau_1 - \tau; \mu, \varphi; \mu_0, \varphi_0) \\ &+ \frac{1}{4\pi\mu} \int_0^1 \int_0^{2\pi} S(\tau_1 - \tau; \mu, \varphi; \mu', \varphi') I(\tau, -\mu', \varphi') \, d\varphi' d\mu', \end{aligned} \tag{8}$$

$$\begin{aligned} I(\tau, -\mu, \varphi) &= \frac{F}{4\mu} T(\tau; \mu, \varphi; \mu_0, \varphi_0) \\ &+ \frac{1}{4\pi\mu} \int_0^1 \int_0^{2\pi} S(\tau; \mu, \varphi; \mu', \varphi') I(\tau, +\mu', \varphi') \, d\varphi' d\mu'. \end{aligned} \tag{9}$$

Equations (6)-(9) yield the scattering and transmission functions in the coupled layers.

The boundary condition on the sea surface is complex because light passing through the sea surface is refracted by the seawater. The relationship between the nadir angle θ_a of the radiation

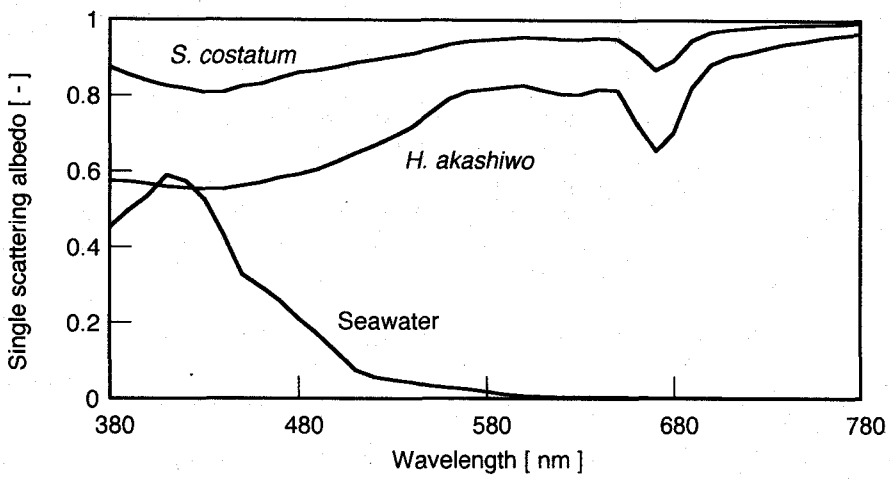

Figure 4. Single scattering albedo of seawater and phytoplankton.

penetrating the atmosphere and that of the ocean, θ_s, can be written by Snell's law as

$$\sin\theta_a = m\sin\theta_s, \quad (10)$$

here m is the refractive index of seawater.

The solid angle of the radiation shrinks when the radiation passes from the atmosphere to the ocean, and it expands from the ocean to the atmosphere. Then, since radiance is represented by solid angle units, the radiance passing the sea surface from the atmosphere to the ocean increases, and from the ocean to the atmosphere it decreases. The increases and decreases in radiance passing the sea surface are corrected by solid angle conversion factors (Tanaka and Nakajima, 1977).

In the radiative transfer model, the sea surface is regarded as one layer, it is assumed to be smooth, and the reflectance and transmittance on the sea surface which varies with the nadir angle of the incident radiation are derived from Fresnel's law of reflection and refraction. The effect of refraction, the shrinking of the solid angle, reflectance, and transmittance are included in reflection and transmission functions in the sea surface layer.

2.2 Model Parameters

The atmosphere has three layers: a boundary layer (sea level-2km), the free troposphere (2-11km) and the stratosphere (11-40km). The ocean has two layers: the surface (sea level-5m depth) and lower layers (5m depth-seafloor). The optical properties of each layer are considered homogeneous; the depth of the seafloor is considered 30m in the coastal zones and 1000m in the open ocean. As sea depth is more than 30m in coastal zones or 1000m in the open ocean, it is possible to neglect the effect of seafloor reflectance on the water-leaving radiance. The zenith angle of the sun is used 43.8°, which is correspondent to the zenith angle of the sun of the Landsat Thematic Mapper image used in chapter 4. The equations of radiative transfer are calculated for the wavelengths 380nm to 780nm at 10nm

Table 1. Optical properties of aerosols in the stratosphere and free troposphere

Aerosol type	r_{gN}	σ_{gN}	β	m_r	m_i
Stratosphere	0.055	2.1	0.004	1.45	1.0E-08
Free troposphere	0.055	2.1	0.025	1.55	0.01

r_{gN} = Geometric number mean radius [μm]
σ_{gN} = Geometric standard deviation
β = Atmospheric turbidity
m_r = real part of refractive index in all calculated wavelength
m_i = imaginary part of refractive index in all calculated wavelength

Table 2. Optical properties of aerosols in a boundary layer

Aerosol type	r_{gN}	σ_{gN}	m_r	m_i	Mass mixing ratio
Elemental carbon	0.055	2.10	1.750	0.550	0.114
Organic carbon	0.055	2.10	1.550	0.000	0.224
Ammonium sulfate	0.055	2.10	1.333	3.24E-09	0.170
Ammonium nitrate	0.055	2.10	1.333	3.24E-09	0.008
Sea solt	0.490	2.15	1.333	3.24E-09	0.403
Soil particles	0.490	2.15	1.550	0.008	0.081

r_{gN} = Geometric number mean radius [μm]
σ_{gN} = Geometric standard deviation
m_r = real part of refractive index (λ = 550nm)
m_i = imaginary part of refractive index (λ = 550nm)

intervals.

The optical properties of the components in each layer are necessary for the calculation of the single scattering albedo, phase function, and optical thickness. The single scattering albedo ω is defined as the ratio of the volume scattering coefficient to the volume extinction coefficient. In satellite remote sensing in the visible region, the radiation transfers through Rayleigh scattering by air or seawater molecules, the Mie scattering by aerosols or suspended substances, and the absorption by dissolved components in the ocean. The phase function of Rayleigh scattering is

$$P_R(\Theta) = \frac{3}{4}(1 + \cos^2\Theta), \quad (11)$$

where Θ is the angle of scattering. The single scattering albedo of air molecules is 1.0 in the visible region, and the optical thickness is given by Young (1981). The scattering by seawater molecules differs slightly from the Rayleigh scattering (Mobley, 1994), but the phase function of seawater molecules is similar to the phase function of air molecules. It was then assumed that seawater molecules cause the Rayleigh scattering. The single scattering albedo of seawater was calculated by using the volume scattering coefficient (Smith and Baker, 1981) and the volume absorption coefficient (Pope and Fry, 1997; Smith and Baker, 1981), and the results are shown in Figure 4. The optical

thickness of seawater is obtained by integrating the volume extinction coefficient from the sea surface to arbitrary depth.

The optical properties of the Mie scattering by aerosols or suspended substances are calculated by using the Mie theory with a complex refractive index and size distribution for these compounds. The optical properties of suspended substances in the ocean are described in the next chapter. In the stratosphere aerosols consist of sulfate particles (Wang *et al.*, 1989) and the complex refractive index of these aerosols are $1.45 - 1\times10^{-8}$i at all calculated wavelengths. In the free troposphere the complex refractive index of aerosols is 1.55 - 0.01i at all calculated wavelengths in the surface and airborne observations of solar radiation flux by Asano (1989). In the boundary layer, aerosols consist of six components: elemental carbon, organic carbon, ammonium sulfate, ammonium nitrate, sea salt, and soil particles (Ohta and Okita, 1990). The fractions of components in aerosols are given by measurements (Ohta *et al.*, 1994; Ohta *et al.*, 1998) and the size distribution of aerosols is presented as log normal. These parameters for the atmosphere are shown in Tables 1 and 2. The optical thickness of the Mie scattering in the atmosphere is given by

$$\tau_M(\lambda) = \beta / \lambda, \quad (12)$$

where β is the atmospheric turbidity coefficient. The values of β in each layer are assumed as 0.004 in the stratosphere, 0.025 in the free troposphere, and 0.15 in the boundary layer (Ohta *et al.*, 1997).

Dissolved organic materials (DOM) in the ocean such as humic acid were considered, and the volume absorption coefficient of DOM is given by

$$a_y(\lambda) = a_y(\lambda_0)\exp[-0.014(\lambda - \lambda_0)]. \quad (13)$$

where λ_0 is a reference wavelength and $a_y(\lambda_0)$ is the absorption coefficient (Mobley, 1994). These values vary with ocean.

3. Optical Properties of Suspended Components in the Ocean

Suspended components in the ocean, phytoplankton, detritus, submicron particles, and inorganic

Table 3. Optical properties of suspended substances in the ocean

Suspended substance type	r_{gN}	σ_{gN}	m_r	m_i
Skeletonema costatum	3.18	0.757	1.041	1.52E-03
Heterosigma akashiwo	5.72	0.905	1.068	2.82E-03
Detritus of *S. costatum*	0.566	0.637	1.047	0
Detritus of *H. akashiwo*	0.542	0.617	1.046	0
Submicron particles	0.21	1.49	1.045	0
Soil particles	0.49	2.15	1.163	0.006

r_{gN} = Geometric number mean radius [μm]
σ_{gN} = Geometric standard deviation
m_r = real part of refractive index (λ = 550nm)
m_i = imaginary part of refractive index (λ = 550nm)

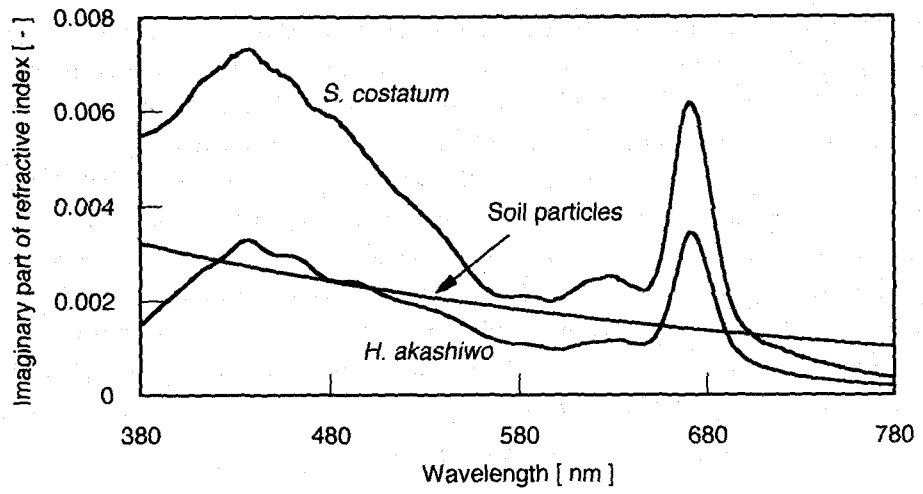

Figure 5. Imaginary part of refractive index of phytoplankton and soil particles

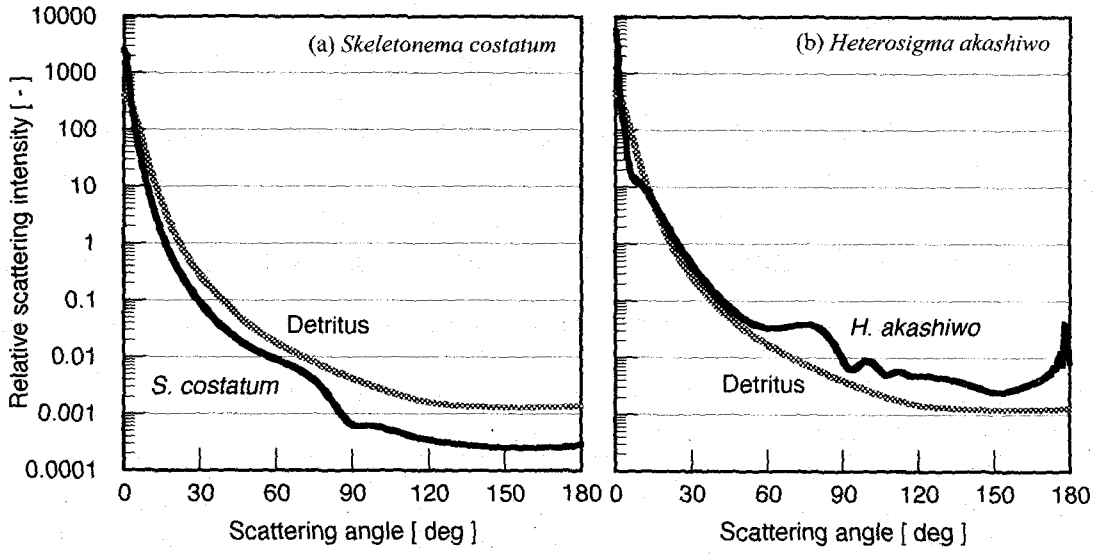

Figure 6. Phase functions of phytoplankton and its detritus at λ=550nm

particles were also considered. The detritus is degraded fragments of phytoplankton, and submicron particles are organic particles with diameters below 1 μm, and the inorganic particles include soil particles and suspended sediment. The complex refractive index and the size distribution

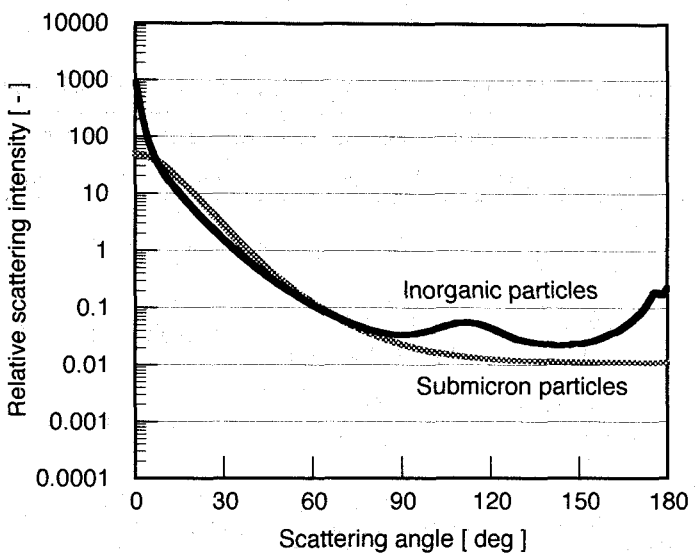

Figure 7. Phase functions of inorganic and submicron particles at λ = 550nm

of phytoplankton and detritus were measured by batch cultured phytoplankton (*Skeletonema costatum*, strain number NIES-16 and *Heterosigma akashiwo*, strain number NIES-4) at NIES (National Institute of Environmental Studies). The size distributions were measured by a microscope with an image processor (Table 3). The real parts of the refractive indices of the phytoplankton and the detritus were determined by immersion refractometry (Jonasz *et al.*, 1997). Table 3 shows the values at 550nm. The imaginary part of the refractive indices of the phytoplankton were calculated with the size distributions and the absorption coefficients measured by a spectrophotometer with a head-on photomultiplier (Bricaud and Morel, 1986). These spectra are shown in Figure 5. The imaginary parts of the refractive indices of the detritus were assumed to be zero. Figure 6 shows the phase functions calculated for *S. costatum* and its detritus, and for *H. akashiwo* and its detritus at 550nm. They show that the phytoplankton, i.e. *S. costatum* and *H. akashiwo*, has very strong forward scattering, and that both kinds of detritus had the same phase function. The single scattering albedos of phytoplankton are shown in Figure 4. They decrease around 450nm and 670nm corresponding to the chlorophyll absorption bands.

It was considered that the submicron particles consist of bacteria and biogenous organic particles. The size distribution of the submicron particles were from observations by Koike *et al.* (1990) and Jonasz *et al.* (1997). The real part of the refractive index of the submicron particles was the average of the observations by Jonasz *et al.* (1997) for bacteria and our measurements for the detritus, which were similar values. The imaginary part of the refractive index of the submicron particles was assumed to be zero. The optical properties of the inorganic particles was estimated from the measured results for *andosol* particles by Meguro (1987). The optical parameters of the submicron particles and the inorganic particles are shown in Table 3. The calculated phase functions at 550nm are shown in Figure 7. Back scattering (at scattering angles of 90-180deg) of these particles is grater than with phytoplankton.

Table 4. Species and concentrarions of suspended substances in each types of waters

Waters type	Concentrations of each suspended substances				DOM
	Phytoplankton	Detritus	Submicron p.	Inorganic p.	$a_y(440)$
Clear waters	*S. costatum* $0.01mg/m^3$	-	$1x10^5$number/ml	-	-
CaseII waters	*S. costatum* $1mg/m^3$	10%v/v of phytoplankton	$1x10^8$number/ml	5mg/l	$0.1m^{-1}$
Turbid waters with soil particles	*S. costatum* $1mg/m^3$	10%v/v of phytoplankton	$1x10^8$number/ml	10-1000mg/l	$0.1m^{-1}$
Red tide waters	*H. akashiwo* $1-100mg/m^3$	50, 200%v/v of phytoplankton	$1x10^8$-$2x10^9$ number/ml	5mg/l	$0.1m^{-1}$

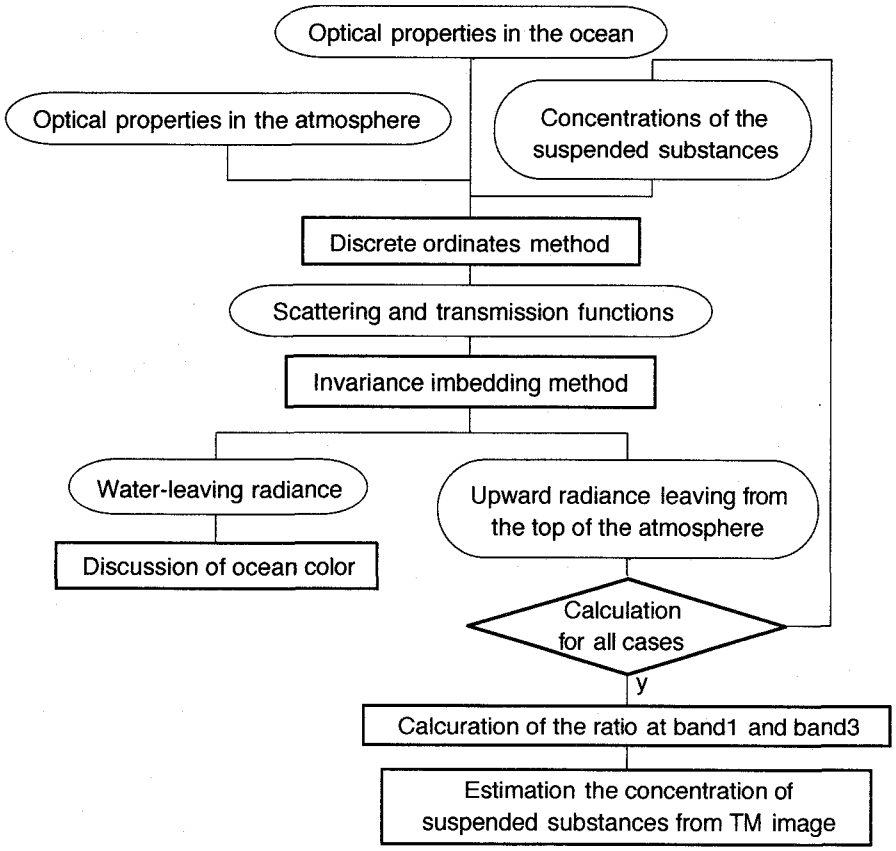

Figure 8. Flowchart of the calculation

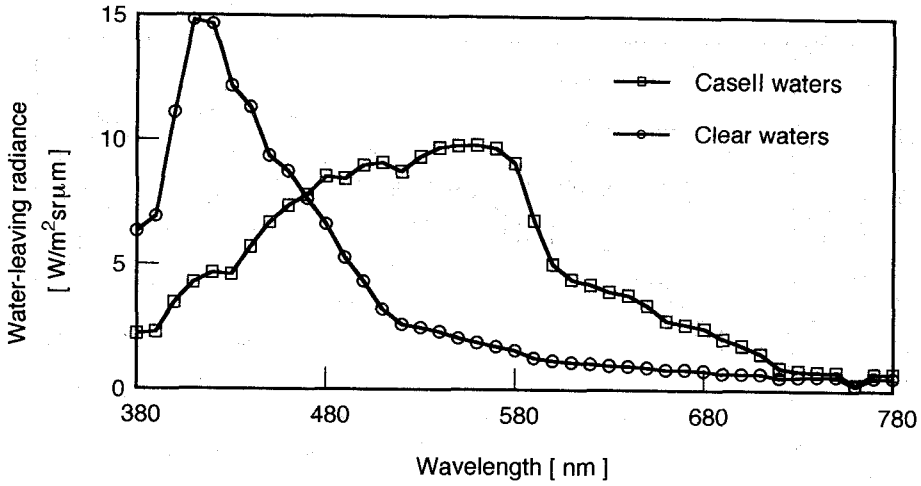

Figure 9. Water-leaving radiance in clear and Case II waters.

4. Calculations of Water-leaving Radiance in Different Types of Water

The spectra of the radiance leaving water and the top of the atmosphere were calculated for different types of waters by using the radiative transfer model for a coupled atmosphere-ocean system. Four types of surface water were considered, clear water, Case II water, turbid water with soil particles, and red tide water. These waters are modeled by varying the species and concentrations as shown in Table 4. The lower water layer is assumed to be Case II water except with clear water. Figure 8 shows the model calculation process.

4.1 Clear and Case II Waters

Clear water, e.g. open ocean water and Kuroshio water, contains only small amounts of suspended compounds such as phytoplankton. Case II water is coastal water, where the concentrations of inorganic particles and dissolved organic matter change the ocean color significantly as well as phytoplankton (Morel and Prieur, 1977). Clear water was assumed to consist of two components, *S. costatum* ($0.01 mg/m^3$) and submicron particles (1×10^5number/ml). Case II water was assumed to consist of five components: *S. costatum*, detritus, submicron particles, inorganic particles, and dissolved organic matter. A typical value for the chlorophyll-a concentration of *S. costatum* was $1 mg/m^3$ for typical Case II waters. The mass of detritus was assumed to be 10% of the phytoplankton. The number of submicron particles observed by Koike *et al.* (1990) was 1×10^8number/ml. The concentration of inorganic particles was 5mg/l. The absorption coefficient of the DOM at 440nm was $a_y(440) = 0.1 m^{-1}$ (Nelson and Guarda, 1995). The calculated spectra of the water-leaving radiance are shown in Figure 9. These spectra agree with the measurements of ocean color by Morel and Prieur (1977). The spectra in clear waters have very strong radiance in the blue region. Because there is little suspended matter in this part of the ocean, the seawater molecules which scatter strongly in the blue

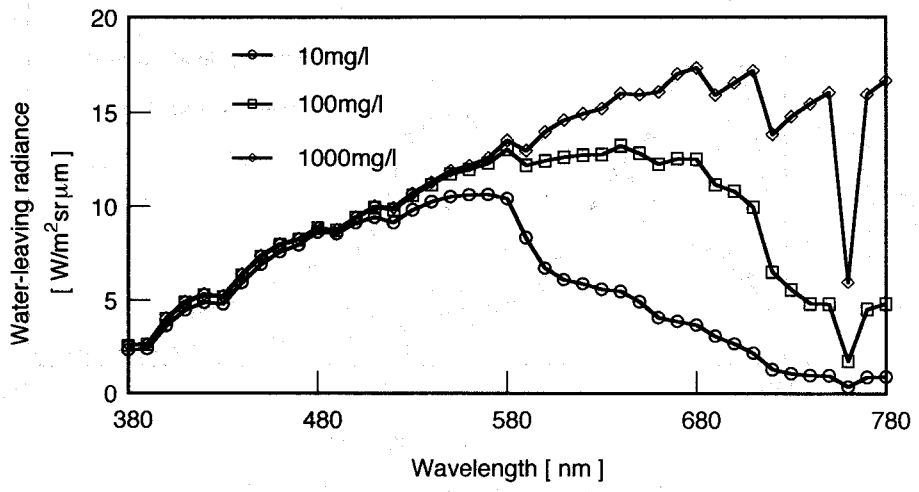

Figure 10. Water-leaving radiance in turbid waters with soil particles for three different mass concentrations.

region (wavelength λ < 500nm) and have high absorptivity in the green and red regions (λ > 500nm), play a major role in the ocean color here. In Case II waters, the spectra have strong radiance in the green region. Since this kind of water contains the highly scattering inorganic particles, the spectrum is strong at all wavelengths. Further, since phytoplankton has high absorptivity in the blue region, the radiance is absorbed at wavelengths shorter than 550nm.

4.2 Turbid Waters with Soil Particles

In turbid waters with soil particles, the optical model parameters were given by the values for Case II waters, except with soil particle concentrations from 10mg/l to 1000mg/l. The optical properties of soil particles are applied to inorganic particles. The calculated spectra of water-leaving radiance are shown in Figure 10 for different soil particle concentrations. The radiance at wavelengths longer than 500nm increases with increases in soil particle concentration, when the ocean color becomes more brown. Soil particles have a high scattering property, and the radiance increases. However, the absorptivity of soil particles at shorter wavelengths is higher than that at longer wavelengths, and the radiance does not increase so much at shorter wavelengths.

4.3 Red Tide Water

It was assumed that red tide water contained five components: red tide phytoplankton, detritus, submicron particles, inorganic particles, and dissolved organic matter. The *H. akashiwo* was considered to form the red tide phytoplankton. The maximum cell number concentration of *H. akashiwo* is 1.35×10^5cells/ml observed by the Kagawa Institute of Red Tides (1994), equivalent to 111mg/m^3 of chlorophyll-a concentration. The red tide phytoplankton concentration was then

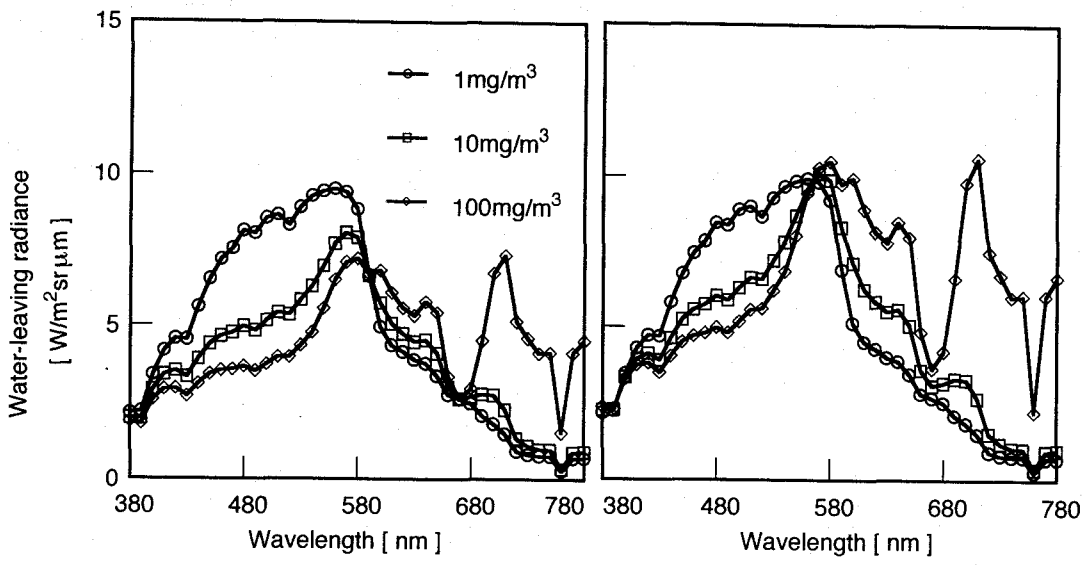

(a) volume ratio of detritus = 50% (b) volume ratio of detritus = 200%

Figure 11. Water-leaving radiance in red tide water for three different phytoplankton concentrations with volume ratios of detritus = 50% and 200%.

considered to range from 1mg/m^3 to 100mg/m^3. The volume of detritus varies with the growth stage of the phytoplankton and was assumed to be 50% and 200% of the volume ratio to the phytoplankton. Koike *et al.*(1990) and Longhurst *et al.*(1992) reported that the submicron particle concentration varies with phytoplankton concentration. The submicron particle concentration then would vary from 1×10^8number/ml to 2×10^9number/ml. The concentration of the inorganic particles is 1mg/l. The absorption coefficient of the DOM at 440nm is $a_y(440) = 0.1\text{m}^{-1}$ (Nelson and Guarda, 1995).

The calculated spectra of water-leaving radiance are shown in Figure 11. With a volume ratio of detritus of 50%, the radiance decreases with increases in the phytoplankton concentration, and the ocean color changes to dark brown. With a volume ratio of detritus of 200%, the radiance increases at wavelengths longer than 570nm with increases in the phytoplankton concentration, and the ocean color of the water changes to light brown. The detritus scatters light more than the phytoplankton. When the ratio of the concentrations of detritus to phytoplankton is low, the radiation penetrates deeper, and is absorbed by the phytoplankton. When the ratio is high, the radiation at wavelengths longer than 570nm, which are little absorbed by the phytoplankton, is scattered upwards by the detritus. When the phytoplankton concentration increases above 100mg/m^3 in both cases, the radiance increases greatly at wavelengths longer than 700nm (the near infrared region), even though the seawater has very high absorptivity in this wavelength region and the water-leaving radiance is usually very weak. This indicates that the scattering effect of phytoplankton and detritus is greater than the effect of absorption by the seawater, and suggests that it would be possible to estimate concentrations of red tide phytoplankton by remote sensors which have high sensitivity in this region.

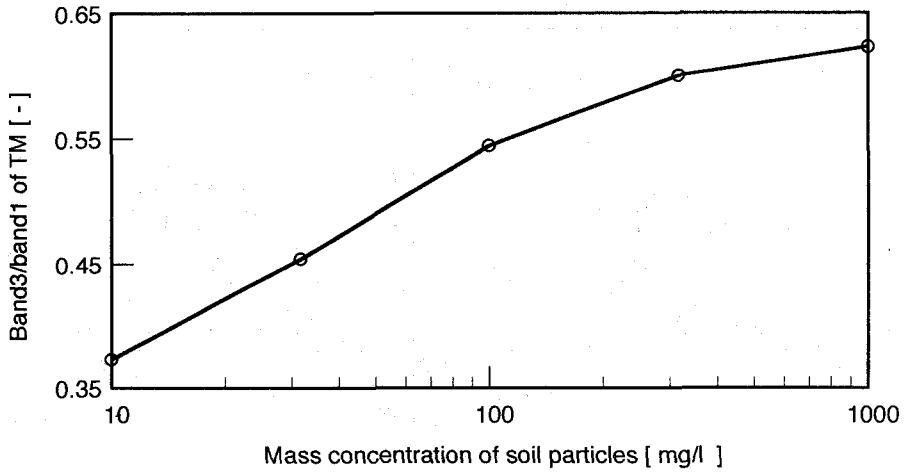

Figure 12. Relationship between the ratio of upward radiance leaving the top of the atmosphere at band1 of the Landsat TM to that at band3 and mass concentrations of soil particle.

5. Remote Sensing for Coastal Pollution

There are numerous sensors and satellites providing observation of the earth. This paper used the Thematic Mapper (TM) of Landsat to evaluate the technique proposed in the paper, as TM has high spatial resolution and sensitivity at blue, green, and red wavelengths. For ocean color remote sensing, it is important to make atmospheric corrections, which derive the water-leaving radiance from the radiance detected by the satellite sensors. The portion of the water-leaving radiance is only a few percent the total observed radiance at the satellite with the rest of the radiance scattered by the atmosphere. In global ocean color remote sensing, it is assumed that the water-leaving radiance in the near infrared region is zero, the radiance detected by the satellite occurs due to atmospheric scattering (e.g. Fukushima *et al.*, 1998). Then, the optical thickness of aerosols is determined by the detected radiance. The radiance scattered by the atmosphere in the visible region is calculated by the optical thickness, and the water-leaving radiance is obtained by subtracting the radiance scattered by the atmosphere from the total observed radiance. In the coastal zone, the water-leaving radiance in the near infrared region is not zero, because there are more suspended substances, such as phytoplankton, and inorganic particles, than in the open ocean. The atmospheric correction for the global ocean is not applicable to the coastal zone. The optical thickness of the aerosols were assumed, and the upward radiance leaving from the top of the atmosphere was used to estimate the suspended matter concentration.

5.1 Algorithm to Estimate Soil Particle Concentrations by TM data

The ratio of the upward radiance leaving the top of the atmosphere at band1 of the TM to that at band3 were calculated with varying the soil particle concentrations. The results are shown in Figure 12,

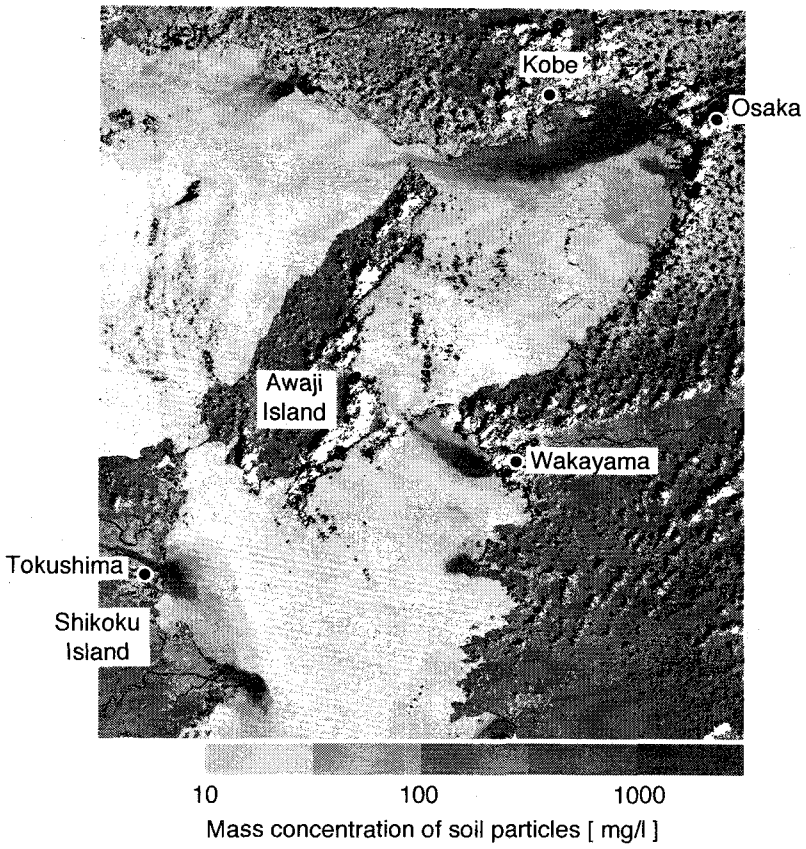

Figure 13. Contour of soil particle concentrations around Osaka bay on September 4, 1989.

the ratio increases with soil particle concentration, and it is possible to determine the soil particle concentration by using TM images.

Figure 13 shows the TM image recording turbid waters with soil particles around Osaka bay on September 4, 1989 (path 110, row 36) from the Remote Sensing Technology Center of Japan (RESTEC). Total precipitation on the day before the image, September 3, 1989, was 121.5mm recorded by the Kobe marine observatory. Figure 13 shows soil particle concentrations calculated by the relation in Figure 12. Figure 13 shows that there are regions where the concentration is over 1000mg/l around the estuaries of rivers and that the flow pattern is affected by tidal currents.

5.2 Algorithm to Estimate Red Tide Phytoplankton Concentrations by TM data

The ratio of upward radiance leaving the top of the atmosphere at band1 of the TM to that at band3 was calculated with varying red tide phytoplankton concentrations. The results are shown in Figure 14. With large amounts of detritus (200%) the ratio increased with concentration, showing that

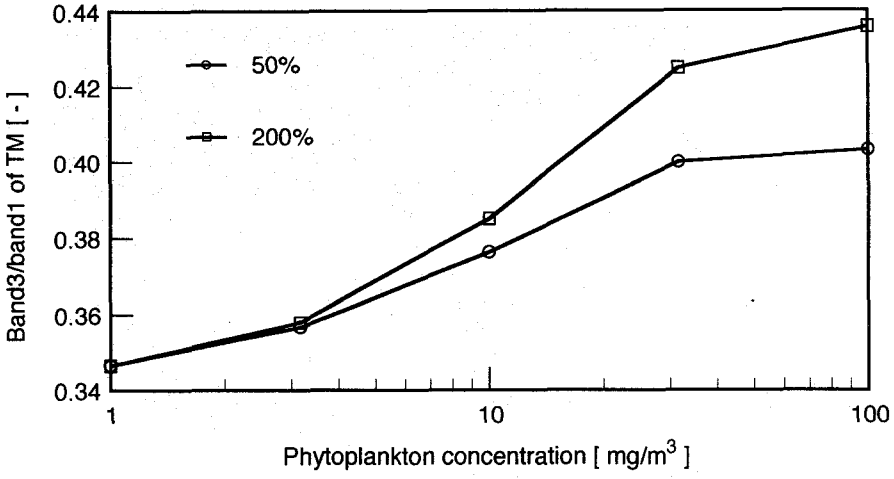

Figure 14. Relationship between the ratio of upward radiances leaving the top of the atmosphere at band1 of the Landsat TM to that at band3 and phytoplankton concentrations with three different detritus ratios.

it is possible to estimate the phytoplankton concentration. With small amounts of detritus, such as at the beginning of red tides, the ratio of upward radiance varies less than with 200% detritus. It is, then, difficult to determine the phytoplankton concentration for this condition.

The accuracy of the ratio between band1 and band3 of the TM was considered. This ratio, R_{13}, is given by

$$R_{13} = \frac{L_3}{L_1}, \quad (14)$$

where L_i is the radiance detected by the sensor and i is the band number. The error in this ratio is δR_{13}, and the total differential of the equation(14) is

$$\delta R_{13} = -\frac{L_3}{L_1^2}\delta L_1 + \frac{1}{L_1}\delta L_3, \quad (15)$$

where δL_i is the error of the radiance detected by the sensors. Dividing equation(15) by equation(14), the relative accuracy of the ratio is given by

$$\frac{\delta R_{13}}{R_{13}} = -\frac{\delta L_1}{L_1} + \frac{\delta L_3}{L_3}, \quad (16)$$

each of δL_1 and δL_3 are independent, and they may assume plus or minus signs. Next the magnitude of the error of the ratio in estimating red tide phytoplankton concentration was estimated. If the red tide phytoplankton concentration is 10mg/m^3 and the detritus ratio is 200%, L_1 = 2.64W/m^{2}sr, L_3 = 1.02W/m^{2}sr, and R_{13} = 0.385. The errors in the radiance detected by the sensor at each band are assumed to the radiance equivalent to 1 digital count of the TM sensor. For example, the magnitude of line noise of TM is 1 digital count or more. The errors of the radiance become δL_1 = 0.0398W/m^{2}sr

and $\delta L_3 = 0.0556 W/m^2sr$, respectively, and the calculated relative accuracy of the ratio is 7.0%, and, $R_{13} = 0.385 \pm 0.027$, a range of 0.358 to 0.412. This range corresponds to the range of the ratio in Figure 14 showing that it is difficult to estimate red tide phytoplankton concentrations using TM data.

6. Conclusions

A radiative transfer model for a coupled atmosphere-ocean system was developed for satellite remote sensing of coastal pollution to estimate the water-leaving radiance from polluted sea surfaces. The radiative transfer equation in the coupled atmosphere-ocean system was solved with the invariance imbedding method. The calculations took account of suspended substances like phytoplankton, detritus, submicron particles, and inorganic particles in the ocean. The optical properties of phytoplankton (*Skeletonema costatum* and *Heterosigma akashiwo*) and its detritus were measured by batch cultured phytoplankton measurements, showing that the phytoplankton has very strong forward scattering. The optical properties of submicron particles and inorganic particles were estimated and it was found that these particles have greater back scattering than phytoplankton.

The spectra of the water-leaving radiance were calculated for several types of waters by solving the equations of radiative transfer in the coupled atmosphere-ocean system. The spectra in clear waters had strong radiance in the blue region, because seawater molecules play the major role in ocean color. In Case II waters, the spectra had strong radiance in the green region, because the water contained inorganic particles that had high scattering in all wavelengths and phytoplankton that had high absorptivity in the blue region. In the turbid waters with soil particles, the water-leaving radiance at wavelengths longer than 500nm increased with increases in soil particle concentration, here the ocean color becomes to browner. In red tide waters, with volume ratios of 50% detritus, the water-leaving radiance decreased with increases of the phytoplankton concentration, here the ocean color becomes to dark brown. With a volume ratio of 200% detritus, the water-leaving radiance at wavelengths longer than 570nm increased with increases in the phytoplankton concentration, here the ocean color changes to light brown. The ocean color in this kind of water thus strongly depends on the amount of detritus.

Algorithms to estimate concentrations of soil particles and red tide phytoplankton by using the Landsat TM data were considered. For the soil particles the ratio of the upward radiance at the band1 wavelength of the TM to that at band3 increases with soil particle concentration, and it is possible to determine the soil particle concentration in this manner. For red tide phytoplankton, the variation in the ratio with concentration increases was very small, and it was difficult to determine the phytoplankton concentration. In this case, two things are necessary. one to use a sensor with a fine quantizing level and high signal to noise ratio to detect small changes of the upward radiance with large increases in red tide phytoplankton concentrations. The other is to use hyper spectral sensors to estimate the phytoplankton concentration and also the detritus concentration. Determining these concentrations in several bands changing independently is necessary. Future studies will develop the algorithm for estimating red tide phytoplankton by hyper spectral sensors.

Acknowledgments

We wish to thank Mayumi Erata of NIES for expert advise on the culturing of phytoplankton. The Landsat TM data was provided by EOSAT/National Space Development Agency of Japan (NASDA) for research, and the data is the property of the government of the United States of America.

References

Asano, S. (1989): Aircraft measurements of the radiative effect of tropospheric aerosols: II. Estimation of aerosol optical properties, J. Meteor. Soc. Japan, Vol.67, pp.1023-1034.

Bricaud, A. and Morel, A. (1986): Light attenuation and scattering by phytoplankton cells:A theoretical modeling, Appl. Opt., Vol.25, pp.571-580.

Chandrasekhar, S. (1960): Radiative Transfer, Dover, pp161-170.

Fukushima, H., Higurashi, A., Mitomi, Y., Nakajima, T., Noguchi, T., Tanaka, T., and Toratani, M. (1998): Correction of atmosphere effect on ADEOS/OCTS ocean color data; Algorithm description and evaluation of its performance, J. Oceanogr., Vol.54, pp.417-430.

Jonasz, M., Fournier, G. and Stramski, D. (1997): Photometric immersion refractometry: a method for determining the refractive index of marine microbial particles from beam attenuation, Appl. Opt., Vol.36, pp.4214-4225.

Koike, I., Hara, S., Terauchi, K. and Kogure, K. (1990): Role of sub-micrometre particles in the ocean, Nature, Vol.345, pp.242-244.

Kagawa institute of red tide (1994): An annual report , Kagawa institute of red tide, pp.4. (In Japanese).

Longhurst, A. R., Koike, I., Li, W.K.W., Rodriguez, J., Dickie, P., Kepay, P., Partensky, F., Bautista, B., Ruiz, J., Wells, M. and Bird, D.F. (1992): Sub-micron particles in northwest Atlantic shelf water, Deep Sea Res., Vol.39, pp.1-7.

Meguro, T. (1987): Measurement of absorption coefficient of soil particles in visible region, Thesis, Hokkaido Univ., Sapporo, Japan. (in Japanese).

Morel, A. and Prieur, L. (1977): Analysis of variations in ocean color, Limnol. Oceanogr., Vol.22, pp.709-722.

Mobley, C. D. (1994): Light and Water, Academic Press, pp102-105.

Nelson, J. R. and Guarda, S. (1995): Particulate and dissolved spectral absorption on the continental shelf of the southeastern United States, J. Geophys. Res., Vol.100, No.C5, pp.8715-8732.

Ohta, S. and Okita, T. (1990): A chemical characterization of atmospheric aerosol in Sapporo, Atmos. Environ., Vol.24A, pp.815-822.

Ohta, S., Murao, N., Yamagata, S. Hayashi, K. and Ishihara, H. (1994): Albedo effect of anthropogenic arctic aerosols on climate, Proc. Environ. Eng. Res., Vol.31, pp.251-262 (in Japanese).

Ohta, S., Murao, N., Yamagata, S. Fukasawa, T., Hasegawa, S. and Arao, K. (1997): Variation in atmospheric turbidity in the area around Japan, J. Global Environ. Eng., Vol.3, pp.9-20.

Ohta, S., Hori, M., Yamagata, S. and Murao, N. (1998): Chemical characterization of atmospheric

fine particles in Sapporo with determination of water content, Atmos. Environ., Vol.32, pp.1021-1025.

Pope, R. M. and Fry, E. S. (1997): Absorption spectrum (380-700nm) of pure water.II. Integrating cavity measurements, Appl. Opt., Vol.36, pp.8710-8723.

Smith, R. C. and Baker, K. S. (1981): Optical properties of the clearest natural waters (200-800nm), Appl. Opt., Vol.24, pp.299-310.

Stamnes, K. (1986): The theory of multiple scattering of radiation in plane parallel atmosphere, Rev. Geophys., Vol.20, pp.177-184.

Tanaka, M. and Nakajima, T. (1977): Effect of oceanic turbidity and index of refraction of hydrosols on the flux of solar radiation in the atmosphere-ocean system, J. Quant. Spectrosc. Radiat. Transfer, Vol.18, pp.93-111

Wang, P. H., McCormick, M. P., Swissler, T. J., Osborn, M. T., Fuller, W. H. and Yue, G. K. (1989): Influence of stratospheric aerosol composition and size distribution from SAGE II satelite measurements, J. Geophys. Res., Vol.94, No.D6, pp.8435-8446.

Young, A. T. (1981): On the Rayleigh scattering optical depth of the atmosphere, Appl. Opt., Vol.20, pp.328-330.